2020-06-01

Decreased motility of flagellated microalgae long-term acclimated to CO2-induced acidified waters

Wang, Y

10.1038/s41558-020-0776-2
Nature Climate Change
Nature Research

Decreased motility of flagellated microalgae grown in CO_2-induced acidified waters for over five years

Yitao Wang[1,2], Xiao Fan[1], Guang Gao[3], John Beardall[3,4], Kazuo Inaba[5], Jason M. Hall-Spencer[5,6], Dong Xu[1], Xiaowen Zhang[1], Wentao Han[1], Andrew McMinn[7] and Naihao Ye[1,2*]

[1]Yellow Sea Fisheries Research Institute, Chinese Academy of Fishery Sciences, Qingdao, China
[2]Function Laboratory for Marine Fisheries Science and Food Production Processes, Qingdao National Laboratory for Marine Science and Technology, Qingdao, China
[3]State Key Laboratory of Marine Environmental Science, Xiamen University, Xiamen 361005, China
[4]School of Biological Sciences, Monash University, Clayton, Victoria 3800, Australia
[5]Shimoda Marine Research Center, University of Tsukuba, Shizuoka, Japan
[6]School of Biological and Marine Sciences, University of Plymouth, PL4 8AA, UK.
[7]Institute of Antarctic and Southern Ocean Studies, University of Tasmania, P.O. Box 252-77, Tasmania 7001, Australia
*E-mail: yenh@ysfri.ac.cn

Motility plays a critical role in algal survival and reproduction, thus affecting the stability of aquatic ecosystems. However, little is known about the effect of elevated CO_2 in marine, brackish and freshwater systems on algal motility. This study used both laboratory microscale and field mesoscale experiments to investigate the motility of three typical phytoplankton species, polar marine *Microglena* sp., euryhaline *Dunaliella salina* and freshwater *Chlamydomonas reinhardtii* grown under different CO_2 concentrations for five years. Motility and the photo-responses of long-term acclimated *Microglena* sp. decreased significantly with increasing CO_2 in all experimental treatments. In a photophobic reaction, changes in intracellular calcium concentration were greatly affected by increasing CO_2. Transcriptomic results showed that genes involved in the regulation of flagellar movement, such as photoreceptor genes, dynein and other axonemal components, were all significantly down-regulated. There was a significant increase in the expression of genes for flagellar shedding under higher CO_2. Parallel experiments with *D. salina* and *C. reinhardtii* showed similar results, suggesting that the observed changes to motility are common across flagellated species. The structure and the bending mechanism of flagella is conserved from unicellular organisms to vertebrates, and thus increases in CO_2 surface water concentrations may affect all flagellated cells exposed to acidified conditions, from algae to fish. Our study suggests that water acidification driven by elevated CO_2 may affect survival and reproduction of organisms with flagella and thus alter the structure and diversity of aquatic ecosystems.

Marine phytoplankton account for nearly 50% of annual global primary productivity[1]. They are the basis of most marine food webs, and provide materials and energy to support complex and productive higher trophic levels[2]. Many phytoplankton migrate vertically on a daily basis to optimize photosynthesis and decrease predation[3]. For many algae, this motion is achieved by the beating of flagella[4]. Unicellular flagellate algae swim towards light by positive phototaxis but if the light is too strong they use photophobic reaction responses to swim away and avoid damage from strong light (negative phototaxis)[5,6].

Here we assess the effects of rising CO_2 levels on movement in a range of algae, because about one third of carbon dioxide released into the atmosphere as a result of human activity has been taken up by surface water masses since the Industrial Revolution, with potential effects on flagellated marine biota. When carbon dioxide dissolves in water it lowers the pH potentially affecting the motility of algae[7,8,9]. Lower pH alters the vertical migration and distribution of *Heterosigma akashiwo*[10], but the effects of CO_2-induced acidification on algal motility are rarely reported, particularly after long-term acclimation.

In our study, three flagellated microalgae, representing different taxa, and originating from different aquatic environments (marine/sea ice habitat, estuarine, freshwater), namely *Microglena* sp. from the Antarctic, the widely distributed euryhalophyte *Dunaliella salina* and the freshwater model microalga *Chlamydomonas reinhardtii*, were investigated. We studied changes in cell motility, as measured by positive and negative phototaxis and responses, at different CO_2 concentrations, including

preindustrial levels, and linked this to gene expression patterns. *Microglena* sp. was cultured at 280, 400, 700, 1000, 1500 and 2000 ppm CO_2 for 5 years and, over the same period, *C. reinhardtii* and *D. salina* were cultured at 400, 1000 and 2000 ppm. In these experiments, we measured both average and instantaneous velocities, representing the ability of microalgae to search for optimal light intensity and quickly escape predators, respectively. We also carried out a field experiment on *Microglena* sp. using natural sunlight to induce positive/negative phototaxis. We address two questions: first, what is the effect of elevated CO_2 on microalgal motility? Secondly, what are the molecular mechanisms that underpin photoreception and motility at the transcriptome level in response to elevated CO_2? We sequenced the entire genome of *Microglena* sp. and provide results from this marine species in the main paper. Our parallel experiments on the brackish water and freshwater flagellates showed the same responses.

As CO_2 levels increased, the average velocity of *Microglena* sp., *C. reinhardtii* and *D. salina* decreased; all the differences were significant at 1000 ppm ($p < 0.05$, Fig. 1a-d, Supplementary Figure 1). Further verification experiments using natural sunlight also showed that the velocity of the algal cells decreased under acidification, and that the decrease was also significant at 1000 ppm ($p < 0.05$, Fig. 1e-h). As shown in Supplementary Figures 2-4, the higher the velocity of the cells, the higher proportion of cell numbers in the movement direction. These results were consistent with the results that are shown in Fig. 1 and Supplementary Figure 1. Measurements of instantaneous velocities also showed similar results to those of average velocities (Supplementary Figures 5-7). Real-time fluorescence images of the cells also reflected

the changes in cell velocity under different pCO_2 (Supplementary Figure 8). Elevated pCO_2 had an adverse effect on cell motility (Supplementary Figure 8). Furthermore, the differential roles of seawater pCO_2 and pH on cell motion were studied. The results showed that the decrease of pH resulted in a significant decrease of cell velocity ($p < 0.05$, Supplementary Figures 9a-d, 10a-d, 11a-d) but the increase of CO_2 without a pH shift had no a significant effect on cell velocity ($p > 0.05$, Supplementary Figures 9e-h, 10e-h, 11e-h).

In the study of positive/negative phototaxis under various CO_2 treatments and different experimental scales, we found that the average velocity of *Microglena* sp., *C. reinhardtii* and *D. salina* showed no significant difference between laboratory microscale and field mesoscale experiments ($p > 0.05$, Supplementary Tables 1-5) except for movement of *Microglena* sp. in the vertical direction under 1500 and 2000 ppm CO_2 (Supplementary Table 1), wherein the velocity of positive phototaxis was significantly higher than the velocity of negative phototaxis ($p < 0.05$). This may be due to buoyancy induced by O_2 released by photosynthesis as our vertical phototaxis response direction was designed to be bottom-up (Supplementary Figures 12a, 13a, 14a).

The effect of positive/negative phototaxis on instantaneous velocity was striking. The positive phototaxis velocity of *Microglena* sp. was significantly higher than that of the negative phototaxis velocity in the both vertical and horizontal directions, except for the horizontal motion under 400 ppm CO_2 ($p < 0.05$, Supplementary Table 6). The positive phototaxis velocity of *C. reinhardtii* and *D. salina* was also significantly higher

than that of the negative phototaxis velocity in the horizontal direction ($p < 0.05$), a result which was similar to that of *Microglena* sp.. However, in the vertical direction, the negative phototaxis velocity of *C. reinhardtii* and *D. salina* was significantly higher than that of the positive phototaxis velocity ($p < 0.05$), except for 2000 ppm treatment of *C. reinhardtii* in the vertical direction (Supplementary Tables 7-8).

Our study shows that elevated CO_2 significantly reduced the instantaneous velocity and average velocity of the cells at both laboratory microscale and field mesoscale levels in *Microglena* sp., *C. reinhardtii* and *D. salina* ($p < 0.05$, Fig. 1 and Supplementary Figures 1, 5, 6, 7). Here we report the analyses of algal photoresponse under blue light, but our results were the same using white light or sunlight (Supplementary Figures 15,16, Supplementary Tables 9-12).

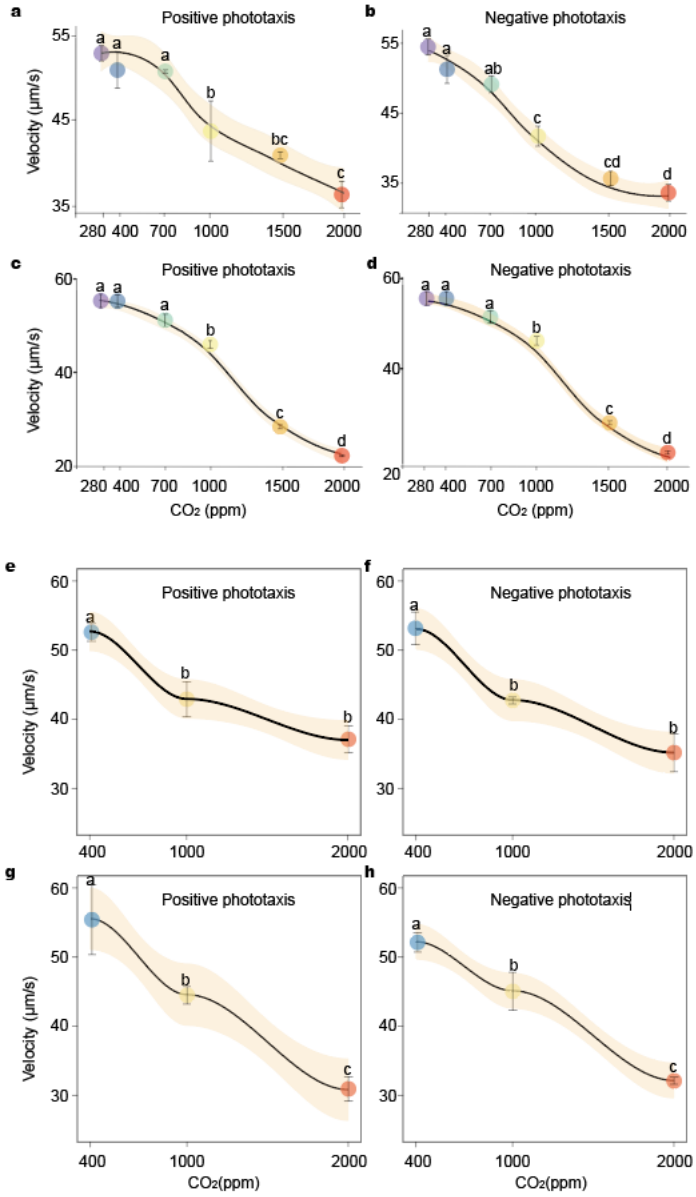

Fig. 1 | Average velocity of *Microglena* sp. induced by artificial light and sunlight in the field. **a**, Positive phototaxis induced by white light in the vertical direction. **b**, Negative phototaxis induced by white light in the vertical direction. **c**, Positive phototaxis induced by white light in the horizontal direction. **d**, Negative phototaxis induced by white light in the horizontal direction. **e**, Positive phototaxis in the vertical direction. **f**, Negative phototaxis in the vertical direction. **g**, Positive phototaxis in the horizontal direction. **h**, Negative phototaxis in the horizontal direction. Curve fitting was performed by a "loose" method using a geometric_smoothing function in the R package "ggplot2". The shaded part represents the 95% confidence interval of the fitted curve. Mean ± SD values per experimental assay are given (n = 3). Different letters in superscript indicate significant differences ($p < 0.05$) among treatments.

There was a significant increase in deflagellation and a decrease in restoration of motility under CO_2-induced acidification (Fig. 2). Long-term CO_2 treatments led to an

increase in the deflagellation ration resulting a decrease in the number of motile cells (Fig. 2a). Increased CO_2 prolonged the recovery time of the proportion of motile cells (Fig. 2b). When CO_2 exceed 1000 ppm, the recovery time of *Microglena* sp. motility was more than 3 hours, significant longer than under 400 ppm ($p < 0.05$, Fig. b-d). This may be related to pH-shock, in which lowering pH induces Ca^{2+}-influx and deflagellation[11]. Non-motile cells without flagella usually sink to the bottom and die under natural conditions[4,12]. Although *Microglena* sp., *C. reinhardtii* and *D. salina* growth increased with acidification in laboratory conditions (Supplementary Figures 17, 18), decreased motility (Fig. 1, Supplementary Figures 1) would likely prove fatal in the natural environment due to a decreased capacity to escape from biotic and abiotic threats. Thus, we predict that under natural conditions, elevated CO_2 will adversely impact the survival of microalgae with flagella.

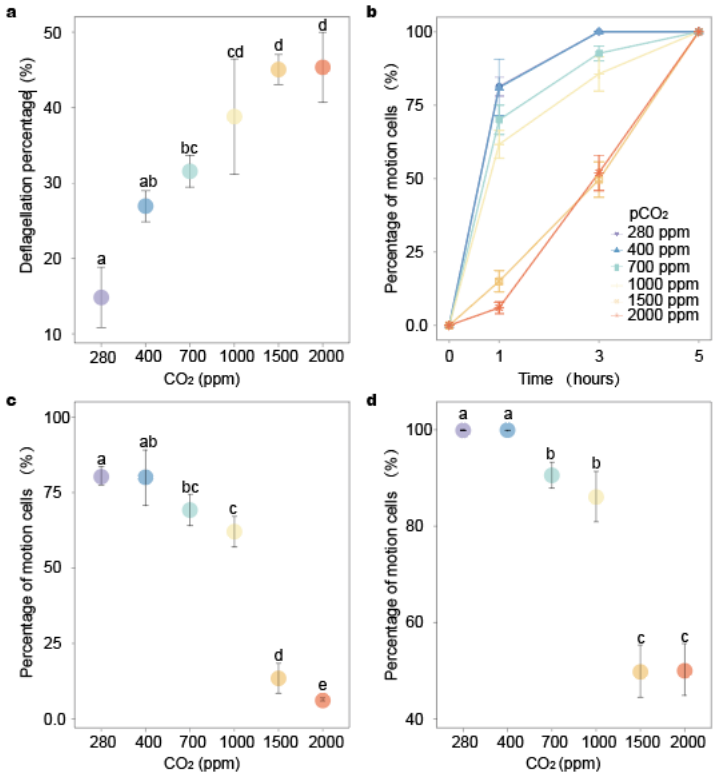

Fig. 2 | CO_2 concentration effects on proportion of *Microglena* sp. showing deflagellation and restoration of motility. a, Deflagellation percentage. **b,** Percentage of motile cells. **c,** Percentage of motile cells after 1 hour. **d,** Percentage of motile cells after 3 hour. Mean ± SD values per experimental assay are given (n = 3). Different letters in superscript indicate significant differences ($p < 0.05$) among treatments.

To clarify the impact of increased CO_2 on flagella, the molecular mechanism by which acidification causes a decrease in swimming velocity was studied in *Microglena* sp. (Fig. 3). We focused on 12 flagella bending genes (Supplementary Table 13) that showed changes in gene expression from transcriptome data and were verified by RT-PCR. Under long-term acidification, transcriptome data showed that genes of *Microglena* sp. which are involved in the initial step for Ca^{2+}-signaling were all down-regulated ($p < 0.05$, Fig. 3f). Genes that promote flagellar motion were all down-regulated in the 1000 ppm CO_2 treatments compared to those in the 400 ppm treatment ($p < 0.05$, Fig. 3d,e). However, CK1 and PKA, which suppress flagellar motion, were significantly up-regulated ($p < 0.05$, Fig. 3e). Furthermore, dynein assembly genes,

DNAAF3/PF22, were down-regulated and deflagellation genes, DIP13/NA14, were up-regulated ($p < 0.05$, Fig. 3c). DC3, a Ca^{2+}-binding component of the dynein-docking complex involved in the dynein assembly, was highly up-regulated ($p < 0.05$, Fig. 3d). The changes in gene expression pattern on acidification in *Microglena* sp. was not restricted to motility gene but occurred on the whole genome level (Supplementary Figure 19). Real-time imaging showed that intracellular Ca^{2+} concentration during positive phototaxis increased, whereas it decreased during negative phototaxis, when the cells were acclimatized to high CO_2 (Fig. 3g, Supplementary Figure 20). These changes were also observed in *C. reinhardtii* and *D. salina* (Supplementary Figure 21).

Given the 5 year length of our experiment, we queried whether genetic modifications had occurred in the algal genome. Illumina WGS was performed for both normal and acidification-treated samples to determine differences in the level of genetic mutations. After mapping c. 240 Gbp reads of normal and acidification-treated samples to the reference genome, it was shown that the overall numbers of SNP (single nucleotide polymorphism) sites were evenly distributed across the genome with a few peaks at specific sites (Supplementary Fig. 22). The normal sample was significantly lower in overall SNPs number compared with the acidified samples (Supplementary Fig. 23). In addition, of all acidified samples, the number of overall SNP sites increased as the CO_2 concentration went up (Supplementary Fig. 23), indicating that acidification was highly impacting on the genetic modifications. Focusing on the relationship between genetic modification and flagellum movement, we specifically studied the SNP profiles of 14 genes directly related to movement. It can be seen from the Supplementary figure 24

that the accumulation of single nucleotide mutations in all the motion-related genes is positively correlated with the degree of acidification （R^2 >>0）. The correlation is significant in 6 of all 14 gene ($P < 0.1$). These genes take their role in motility, phosphorylation and dynein assembly, indicating the genetic adaptation of motility to the oceanic acidification. In order to investigate the effect of genetic mutations on codons, we calculated the synonymous mutation rate and the non-synonymous mutation rate of motion-related genes (Supplementary Figure 25). We found Ka are generally less than Ks when compared in 400 ppm ($p<0.05$), indicating more mutations do not cause changes in the coding protein in the normal acidification. However, the difference does not exist in 1000 ppm and 2000 ppm. This indicates that with the increase of acidification gradient, more non-synonymous mutations will occur, thus accelerating the selection effect of environment on individual genes. This conjecture is supported somewhat by another diagram. We found that the median value of Ka/Ks climb as acidification increased, however it is not significant.

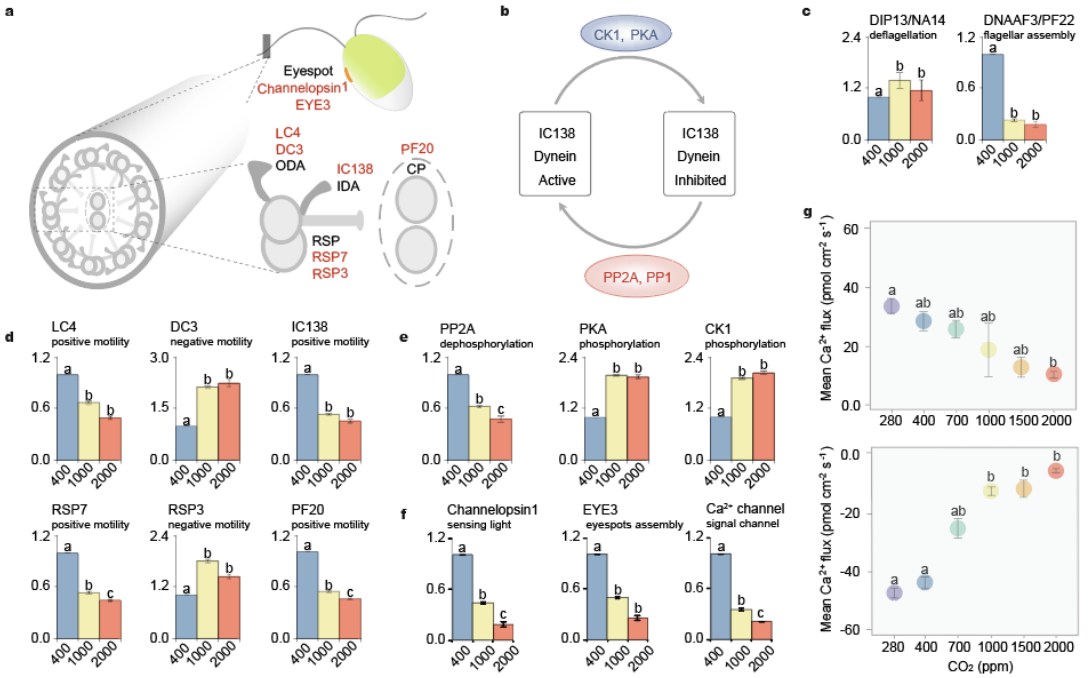

Fig. 3 | Changes in the expression of motility-related genes. a, Schematic diagram of light sensation and Ca^{2+} - mediated flagellar beating in *Microglena* sp.. ODA, outer dynein arm. IDA, inner dynein arm. RSP, radial spoke protein. CP, central pair apparatus. The genes for RT-PCR are listed in red. **b,** Regulation of an inner dynein arm by the phosphorylation/dephosphorylation of IC138 via protein kinases and phosphatases. **c,** Changes of gene expression for deflagellation and flagellar assembly under the 1000 and 2000 ppm treatments relative to the 400 ppm treatment. **d,** Changes of gene expression for dynein subunits under the 1000 and 2000 ppm treatments relative to the 400 ppm treatment. **e,** Changes of gene expression for the regulation of IC138 under the 1000 and 2000 ppm treatments relative to the 400ppm treatment. **f,** Changes of gene expression for eye-spot and Ca^{2+}-regulation under the 1000 and 2000 ppm treatments relative to the 400ppm treatment. **g,** the mean flux of Ca^{2+} under different pCO_2 scenarios. Mean ± SD values per experimental assay are given (n = 3). Upper, Ca^{2+} efflux under positive phototaxis. Lower, Ca^{2+} influx under negative phototaxis, "-" on the vertical scale means Ca^{2+} entry. LC4, flagellar outer dynein arm light chain 4; DC3, outer dynein arm docking complex protein 3; IC138, a 138 kDa intermediate chain of I1/f inner arm dynein; RSP, radial spoke protein; PF20, a protein of the central pair apparatus; PKA, cAMP-dependent protein kinase; PP2A, protein phosphatase 2A; CK1, casein kinase 1; DIP13/NA14, deflagellation inducible protein; DNAAF3/PF22, axonemal dynein assembly factor. Mean ± SD values per experimental assay are given (n = 3). Different letters in superscript indicate significant differences ($p < 0.05$) among treatments.

The phototactic pathway of *Microglena* sp. is not fully understood. Due to the highly-conserved structure of the flagellum and similarity of photosensitive organs of flagellated green microalgae, *C. reinhardtii* was used to annotate flagellate-related genes in the *Microglena* sp. motility-related genes, so the existing *C. reinhardtii*

227 pathway was used to study the *Microglena* sp. motility-related genes. The phototactic
228 pathway of *Chlamydomonas* primarily consists of three steps: (i) a light inward current
229 in the eyespot, which functions as a light reflector and light-gated ion channel[11]. (ii) a
230 photocurrent depolarized activated voltage-gated Ca^{2+} channel in flagella[5,11,13]. (iii)
231 flagellar bending stimulated by Ca^{2+} and inhibited by cAMP[5]. Flagellar beat is driven
232 by the axonemal dyneins, which are regulated by Ca^{2+} -binding proteins LC4, DC3[11]
233 and a phosphorylation protein IC138. The components of radial spokes and central pair
234 apparatus also play a significant role in regulating axonemal dyneins[5,11,13,14,15]. The
235 present study shows that long-term acidification negatively affected expression of
236 genes related to photosensitivity, signal transduction and the regulation of dyneins and
237 flagellar motility (Fig. 3). In addition, the acidification resulted in decreased formation
238 and stability of flagella (Fig. 3c). Taken together, these results suggest that long-term
239 exposure to acidification has negative effects on the motility of *Microglena* sp..
240 Under the business as usual emissions scenario (RCP8.5, IPCC 2019), Antarctic
241 terrestrial ice-free areas could increase by close to 25% by the end of the century,
242 causing fundamental changes to the region[16]. Changes in phytoplankton species
243 composition and the seasonality of production affect Antarctic food webs and are
244 induced by the retreat of winter sea ice[17]. As a polar alga, *Microglena* sp. will be
245 affected by both sea ice loss and acidification, since its light compensation point is
246 reduced under ocean acidification (Fig. 4a).

247 *Microglena* sp. survives under sea ice all year round[18]. Due to the strong attenuation
248 of natural light through the ice, light intensity under the ice is much lower than in non-

ice-covered waters[9] and *Microglena* sp. is well adapted to an under-ice, low light environment[18]. When sea ice melts, accelerated by climate change, *Microglena* sp. is exposed to much greater light intensities. Consequently, the vertical migration distance increases if cells are to position themselves in a region of appropriate light intensity (Fig. 4). As shown in Fig. 4c, we calculated how much time it would take *Microglena* sp. to cover the DVM using the average and instantaneous velocities under positive/negative phototactic responses. Under positive phototaxis, at 2000 ppm, the average velocity is 0.13 m/h and the instantaneous velocity is 0.29 m/h. It would take *Microglena* sp. 2.57-5.65 days to cross the DVM. For *Microglena* sp. adapted to 280 ppm, it would take 14.64 h, to 1.89 days. It also takes show an extended period of time to cross the DVM under increased CO_2 during the negative phototaxis response. However, an increase in ocean acidification will decrease the motility of *Microglena* sp., which we suspect will put this organism at a disadvantage such that it will likely be outcompeted in ice-free conditions, changing the Antarctic ecosystem. *C. reinhardtii* and *D. salina*, which are not protected by ice, experience dramatic changes in the light in their environment. In this case, the cells can escape light stress through motility. Prolonged exposure to bright light increases the risk of light damage and increasing CO_2 concentrations decreased cells motility, which can lead to prolonged exposure to high light stress and thus increase the risk of photo-damage. At the same time, weakened motility will make it harder for cells to escape predators[4,12].

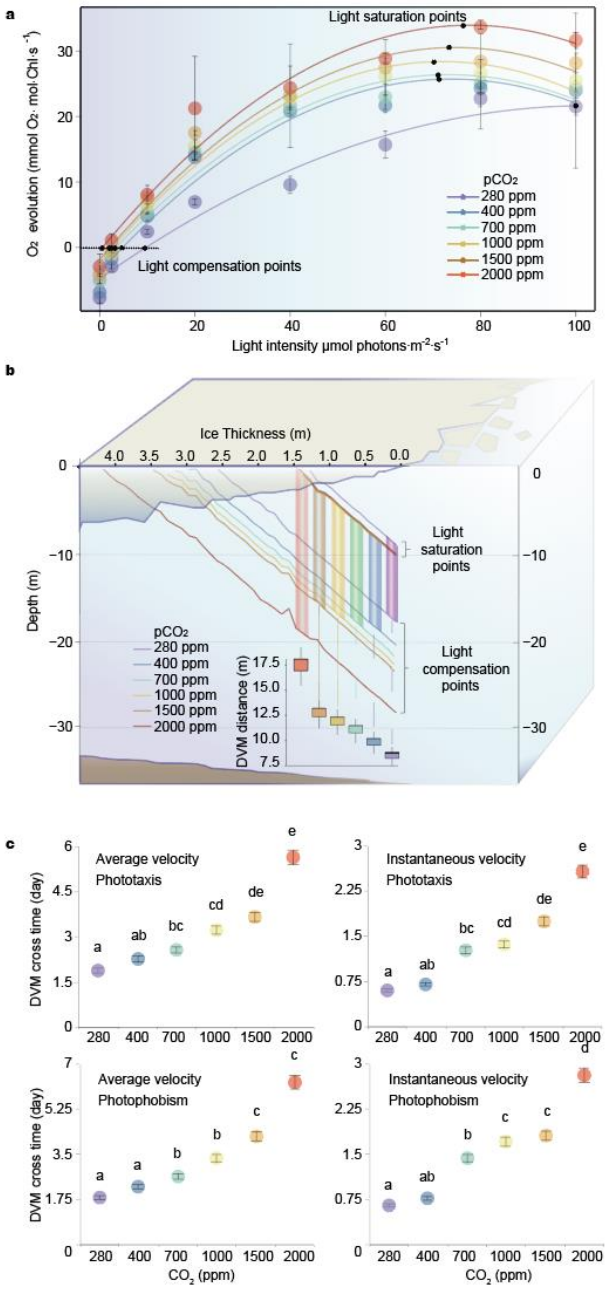

Fig. 4 | Distribution of *Microglena* sp. and light intensity under melting ice. **a**, Photosynthetic light curve of *Microglena* sp. under different CO_2 concentrations. Mean ± SD values per experimental assay are given (n = 3). **b**, The incident light distribution in the water under melting ice. Upper and lower horizontal lines represent saturating light intensity and the light compensation point respectively. *Microglena* sp. lives between the saturated and compensation isophotic lines and moves corresponding to the solar cycle. *Microglena* sp. Daily Vertical Migration (DVM) distance was defined as the vertical distance between the water layer where the light compensation point of algae was located and the water layer where the saturation point was located. **c**, *Microglena* sp. cover the DVM time using the average and instantaneous velocities under positive and negative phototaix. Upper left, positive phototaxis using average velocity. Upper right, positive phototaxis using instantaneous velocity. Lower left, negative phototaxis using average velocity. Lower right, negative phototaxis using instantaneous velocity.

There is growing concern for how biodiversity loss due to human-induced environmental change will affect the functioning of ecosystems and, in turn, the services ecosystems provide to human beings[19,20]. The influence of elevated pCO_2 on the species biodiversity and richness of the phytoplankton assemblages could be profound, through negative effects on some organisms and changes to biogenic habitat[21]. Our study shows, both at physiological and gene-expression levels, that elevated CO_2 concentration significantly decreases the motility of three typical microalgae after a five-year acclimation, which would impact their reproduction and survival, and thus the abundance of microalgae with flagella in aquatic ecosystem. Given that the structure and motility regulation of eukaryotic cilia and flagella are evolutionary conserved[6,22,23], our study reveals the potential effects of aquatic acidification on a wide range of cilia and flagella in eukaryotic organisms, including sperm motility and fertilization[12], cilia-based epithelial fluid flow and the determination of left–right asymmetry[6].

REFERENCES

1. Field, C. B., Behrenfeld, M. J., Randerson, J. T., & Falkowski, P. Primary production of the biosphere: integrating terrestrial and oceanic components. *Science* **281**, 237-240 (1998).
2. Ullah, H., Nagelkerken, I., Goldenberg, S.U. & Fordham, D.A. Climate change could drive marine food web collapse through altered trophic flows and cyanobacterial proliferation. *PLOS Biol.* **16**, e2003446 (2018).
3. Hall, N.S. & Paerl, H.W. Vertical migration patterns of phytoflagellates in relation to light and nutrient availability in a shallow microtidal estuary. *Mar. Ecol. Prog. Ser.* **425**, 7-21 (2015).
4. Stocker, R. & Durham, W.M. Tumbling for Stealth? *Science* **325**, 400-402 (2009).
5. Sineshchekov, O.A., K.H. Jung, & Spudich, J.L. Two rhodopsins mediate phototaxis to low- and high-intensity light in *Chlamydomonas reinhardtii*. *P. Natl. Acad. Sci. USA* **99**, 8689-8694 (2002).
6. Elgeti, J. Winkler, R.G. & Gompper, G. Physics of microswimmers—single particle motion and collective behavior: a review. *Rep. Prog. Phys.* **78**, 1-50 (2015).
7. Caldeira, K. & Wickett M.E. Anthropogenic carbon and ocean pH. *Nature* **425**, 365 (2003).

8. Flynn, K.J., Blackford, J.C., Baird, M.E., Raven, J.A., Clark, D.R., Beardall, J., Brownlee, C., Fabian, H., & Wheeler, G.L. Changes in pH at the exterior surface of plankton with ocean acidification. *Nat. Clim. Change* **2**, 510-513 (2012).
9. Assmy, P., Fernández-Méndez, M., Duarte, P. & Meyer, A. Leads in Arctic pack ice enable early phytoplankton blooms below snow-covered sea ice. *Sci. Rep-UK* **7**, 40850 (2017).
10. Kim, H., Spivack, A.J. & Menden-Deuer S. pH alters the swimming behaviors of the raphidophyte *Heterosigma akashiwo*: Implications for bloom formation in an acidified ocean. *Harmful Algae* **26**, 1-11 (2013).
11. Wheeler, G.L. Calcium-Dependent signalling processes in *Chlamydomonas*. *Chlamydomonas: Molecular Genetics and Physiology*. (eds Hippler, M.) 233-255 (Springer, Cham, Heidelberg 2017).
12. Waisbord, N. & Guasto, J.S. Peculiar polygonal paths. *Nat. Phys.* **14**, 1157-1162 (2018).
13. Uekia, N.& Wakabayashi, K. Detergent-extracted *Volvox* model exhibits an anterior–posterior gradient in flagellar Ca^{2+} sensitivity. *P. Natl. Acad. Sci. USA* **115**, E1061-E1068 (2018).
14. Yang, X.L., Xu, H., Li, D., Gao, X., Li, T.L. & Wang, R. Effect of melatonin priming on photosynthetic capacity of tomato leaves under low-temperature stress. *Photosynthetica* **56**, 884-892 (2018).
15. Indaba, K. Sperm flagella: comparative and phylogenetic perspectives of protein components. *MHR: Basic Sci. of Reprod. Med.* **17**, 524-538 (2011)
16. Shikata, T., Matsunaga, S., Nishide, H., Sakamoto, S., Onistuka, G. & Yamaguchi, M. Diurnal vertical migration rhythms and their photoresponse in four phytoflagellates causing harmful algal blooms. *Limnol. Oceanogr*. **60**, 1251-1264 (2015).
17. Smetacek, V. & Nicol, S. Polar ocean ecosystems in a changing world. *Nature* **437**, 362-368 (2005).
18. Raymond, J.A. & Morgan-Kiss, R. Multiple ice-binding proteins of probable prokaryotic origin in an Antarctic lake alga, *Chlamydomonas* sp. ice-mdv (Chlorophyceae). *J. Phycol.* **53**, 848–854 (2017).
19. Duffy, J.E., Godwin, C.M. & Cardinale, B. J. Biodiversity effects in the wild are common and as strong as key drivers of productivity. *Nature* **549**, 261 (2017).
20. Hall-Spencer, J. M., & Harvey, B. P. Ocean acidification impacts on coastal ecosystem services due to habitat degradation. *Emerg. Top. in Life Sci.*, **3**, 197-206 (2019).
21. Sunday, J.M., Fabricius, K.E., Kroeker, K.J. & Anderson, K.M. Ocean acidification can mediate biodiversity shifts by changing biogenic habitat. *Nat. Clim. Change* **7**, 81 (2017).
22. Jeanneret, R., Contino, M. & Polin M. A brief introduction to the model microswimmer *Chlamydomonas reinhardtii*. *Eur. Phys. J. Spec. Top*. **225**, 2141-2156 (2016).
23. Indaba, K. & Mizuno, K. Sperm dysfunction and ciliopathy. *Reprod. Med. Biol.* **15,** 77-94 (2016).
24. Platt. T., Gallagos. C.C. & Hamson. W. G Photoinhibition of photosynthesis in natural assemblages of marine phytoplankton. *J. Mar Res.* **38**, 687-701 (1980).
25. Li, Y., Horsman, M., Wang, B., Wu, N., & Lan, C. Q. Effects of nitrogen sources on cell growth and lipid accumulation of green alga Neochloris oleoabundans. *Appl. Microbial. Biot.*, **81**, 629-636 (2008).
26. Lichtenthaler, H.K. Chlorolphylls and Carotenoids: Pigments of Photosynthetic Biomembranes. *Method. Enzymo.* **148**, 350-382 (1987).
27. Sueltemeyer, D.F., Klug, K. & Fock, H.P. Effect of photon fluence rate on oxygen evolution and

uptake by *Chlamydomonas reinhardtii* suspensions grown in ambient and CO_2-enriched air. *Plant Physiol.* **81**, 372-375 (1986).
28. Rühle, T., Hemschemeier, A., Melis, A. & Happe, T. A novel screening protocol for the isolation of hydrogen producing *Chlamydomonas reinhardtii* strains. BMC Plant Biol. **8**, 107 (2008).
29. Siiltemeyer, D.F., Klock, G., Kreuzberg, K. & Fock, H.P. Photosynthesis and apparent affinity for dissolved inorganic carbon by cells and chloroplasts of *Chlamydomonas reinhardtii* grown at high and low CO_2 concentrations. *Planta* **176**, 256-260 (1988).
30. Ueki, N., Ide, T., Mochiji, S., Kobayashi, Y. & Tokutsu, R. Eyespot-dependent determination of the phototactic sign in *Chlamydomonas reinhardtii*. *P. Natl. Acad. Sci. USA* **113**, 5299-5304 (2016).
30. SooHoo, J.B., Palmisano, A.C., Kottmeier, S.T., Lizotte, M., SooHoo, S.L. & Sullivan, C. Spectral light absorption and quantum yield of photosynthesis in sea ice microalgae and a bloom of *Phaeocystis pouchetii*. *Mar. Ecol-Prog. Ser.* **39**, 175-189 (1987).
31. Sun, J., Wang, M.J., Ding, M.Q., Deng, S.R., Liu, M.Q., Lu, C.F., Zhou, X.Y., Shen, X., Zheng, X.J., Zhang, Z.K., Song, J., Hu, Z.M., Xu Y. & Chen S.L. H_2O_2 and cytosolic Ca^{2+} signals triggered by the PM H^+-coupled transport system mediate K^+/Na^+ homeostasis in NaCl-stressed *Populus euphratica* cells. *Plant Cell Environ.* **33**, 943-958 (2010).

Acknowledgements This work was supported by the national key re-search and development program of China (2018YFD0900703, 2016YFC1402102, 2018YFD0901503-8), Marine S&T Fund of Shandong Province for Pilot National Laboratory for Marine Science and Technology (Qingdao) (NO. 2018SDKJ0406-3); Financial Fund of the Ministry of Agriculture and Rural Affairs, P. R. of China (NFZX2018). Projects of International Exchange and Cooperation in Agriculture, Ministry of Agriculture and Rural Affairs of China- Science, Technology and Innovation Cooperation in Aquaculture with Tropical Countries along the Belt and Road; Shandong key Research and Development Plan (2018GHY115010); National Natural Science Foundation of China (41676145); China Agriculture Research System (CARS-50); Central Public-interest Scientific Institution Basal Research Fund, YSFRI, CAFS (20603022016001, 20603022019006); Taishan Scholars Funding of Shandong Province; Talent Projects of Distinguished Scientific Scholars in Agriculture.

Author contributions N.H.Y. designed the project. Y.T.W., D.X., X.W.Z. and W.T.H performed the research. F.X., N.H.Y., and Y.T.W. analyzed the data. Y.T.W. and N.H.Y. wrote the first draft and all authors contributed to interpreting the data and writing the manuscript. The authors declare no conflict of interest.

METHODS

Cell Culture. *Microglena* sp., *Chlamydomonas reinhardtii* and *Dunaliella salina* acquired from Yellow Sea Fisheries Research Institute were used in this study. These three species were semi-continuously cultured in aerated 500 ml conical flasks containing 400 ml of medium (Supplementary Table 2, 3, 4) in a 12-h/12-h light/dark cycle and at 6℃, 20℃, 20℃, respectively.

Microglena sp. was cultured in a series of CO_2 treatments (280, 400, 700, 1000, 1500, 2000 ppm), coded as "M_{280}", "M_{400}", "M_{700}", "M_{1000}", "M_{1500}", "M_{2000}", respectively. *C. reinhardtii* was cultured in three CO_2 treatments (400, 1000, 2000 ppm), coded as "CR_{400}", "CR_{1000}", "CR_{2000}",

respectively. *D. salina* was also cultured in three CO_2 treatments (400, 1000, 2000 ppm) coded as "DS_{400}", "DS_{1000}", "DS_{2000}", respectively. The ambient CO_2 concentration of 400 ppm was designated the control treatment. All cultures (Supplementary Table 14-16) were conducted in CO_2 plant incubators (HP-1000, Ruihua, China) to maintain the stability of CO_2 and the variations of CO_2 was shown in Supplementary Tables 17-20. The pH in each culture was monitored once every day using a portable pH electrode (6010M, Jenco, USA) to ensure the stability of the pH level during the culture period (Supplementary Tables 17-18). All following experiment assays were performed using cells in the light period (6∼8 h after the light came on) after the five-year acclimation.

Photosynthesis vs light curve. For each sample, oxygen production and oxygen uptake were obtained at 6 °C using 4 mL respiration chambers fitted with micro-probes, glass-coated stir bars, Clark-type OX-MR oxygen microsensors and a PA 2000 picoammeter, and data logged using MicOx 2.6 data acquisition software (Microrespiration system, Unisense). Oxygen microsensors were polarized continuously for > 24 hours before use. Oxygen production and oxygen uptake ratio were recorded at different light intensities using LEDs and then fitted to the relationships described by Platt *et al*. (1980)[24]（Supplementary Table 21）. The intersection point between the photosynthetic oxygen release curve and the X-axis is the light compensation point, and the point when the photosynthetic oxygen release reaches its maximum value is the light saturation point.

Chlorophyll determination. Chlorophyll measurement Fresh algal cells collected in a 2ml centrifuge tube from 2ml cultivated broth by centrifuge were disrupted in an ultrasonic bath (KQ3200DA, Kunshan, China) in ice bath for 45 min and extracted with 2 ml 95% ethanol overnight in 4℃. The extractant was centrifuged at 3,000×*g* for 5 min[25]. The chlorophyll content was determined spectrophotometrically as follows:

Chl =$5.24A_{664.2} + 22.24A_{648.6}$, where $A_{664.2}$ and $A_{648.6}$ represent absorbance of the methanol extracts at 664.2 and 648.6 nm, respectively[26].

Light intensity for positive and negative phototaxis. Phototaxis is the biological tendency to move under light stimulation. Positive phototaxis occurs when algae sense light through the eyespot and move toward it through their motor organs. Negative phototaxis is a reaction of algae to sense light through the eyespot and away from it through their motor organs. Compared with *C. reinhardtii*, *Microglena* sp. had a very low light compensation point (4.8 μmol photons·m^{-2}·s^{-1}) and saturation points (73.82 μmol photons·m^{-2}·s^{-1}), which is about 10% that of *C. reinhardtii* under normal conditions (Fig. 4a). Light density distribution with variations in incident irradiance were measured during the positive/negative phototaxis assays of *Microglena* sp., *C. reinhardtii* and *D. salina* (Supplementary Figure 12, 13). Consequently, irradiances of 2 μmol photons·m^{-2}·s^{-1} and 200 μmol photons·m^{-2}·s^{-1} were selected as the positive phototaxis-inducing light and negative phototaxis-inducing light respectively. For *C. reinhardtii* and *D. salina*, the positive phototaxis-inducing light was the same as that induced by *Microglena* sp. and negative phototaxis-inducing light was 800 μmol photons·m^{-2}·s^{-1} [27-29].

Vertical cell motion. Cells were washed with pre-acidified experimental solution with different pCO_2 and kept under red light for more than 50 min before the assays[30]. In all the experiments involving light induction, we use a customized LED light source with multiple lamp beads, which can emit parallel light of wavelengths of 400-700 nm and with the light intensity adjustable in the range of 0-2000 μmol photons·m^{-2}·s^{-1}. For vertical laboratory microscale experiments, the acrylic channel used had an inner diameter of 4.4 cm and a height of 11 cm (Supplementary Figure 12a,

14a). In order to maintain the stability of the acrylic channel, in the outdoor experiment, we extended the length of the acrylic channel to 40 cm and used only the top 11cm during mesoscale experiments (Supplementary Figure 13a). For the positive phototaxis assays, 15 mL cell suspensions (~2.4x10^6 cells/mL) were placed into the bottom of acrylic channels by a pipette, illuminated with a LED (White/Blue, ~2 μmol photons·m^{-2}·s^{-1}) from immediately above for 20 min and sampled every centimeter (Supplementary Figures 14a). For the negative phototaxis assays, 15 mL cell suspensions (~2.4x10^6 cells/mL) were placed into the top of the acrylic channels by a pipette, illuminated with a LED (White/Blue, ~200 μmol photons·m^{-2}·s^{-1}/~800 μmol photons·m^{-2}·s^{-1}) from immediately above for 20 min, and sampled every centimeter (Supplementary Figures 14a). The positive phototaxis assay treatment was used to keep cells at the top of the vessel during the negative phototaxis assays. To calculate the cell velocity, we chose the average distance from the sampling point to the loading point (as a point without volume) as the distance of the cells had moved at each sampling point. The distance moved was set to 0.5, 1.5, 2.5, 3.5, 4.5, 5.5, 6.5, 7.5, 8.5, 9.5 cm corresponding to samples from 1 to 10, respectively. The average velocity was calculated as follows:

Velocity = ($C_1V_1xS_1$+ $C_2xV_2xS_2$+……+ $C_{10}xV_{10}xS_{10}$) /t / (C_1xV_1 + C_2xV_2 +… …+ $C_{10}xV_{10}$) (Equation 1)

C: cell concentration; V: sample volume; S: distance moved; t: move time.

Horizontal cell motion. Cells were washed with a pre-acidified experimental solution with different CO_2 concentrations and kept under red light for more than 50 min before the assays. For horizontal laboratory microscale experiments, the acrylic channel was oblong with a square cross section with each side being 4 cm, and channels were evenly divided into 11 parts with a width of 1cm each (Supplementary Figure 12b, 14b). As for the vertical cell motion study, in order to maintain the stability of the acrylic channel, in the outdoor experiment, we extended the length of the acrylic channel to 40 cm and used 11 cm on one end during mesoscale experiments (Supplementary Figure 13d). For the positive phototaxis assays, 15 mL cell suspensions (~2.4x10^6 cells/mL) were placed into one side of the acrylic channels, matching acrylic cards were inserted to separate the cell suspensions after illuminating with a LED (White, ~2 μmol photons·m^{-2}·s^{-1}) from the opposite side for 20 min and sampled every centimeter (Supplementary Figures 14b). For the negative phototaxis assays, 15 mL cell suspensions (~2.4 × 10^6 cells/mL) were placed into one side of acrylic channels, illuminated with a LED (White, ~200 μmol photons·m^{-2}·s^{-1}/~800 μmol photons·m^{-2}·s^{-1}) from side for 20 min, and sampled every centimeter (Supplementary Figures 14b). To calculate the cell velocity, we chose the average distance from the sampling point to the loading point (as a point without volume) as the distance of the cells at each sampling point. The distance moved was set to 0.5, 1.5, 2.5, 3.5, 4.5, 5.5, 6.5, 7.5, 8.5, 9.5 cm corresponding to samples from 1 to 10, respectively. The average velocity was calculated as in Equation 1.

Field experiment. To further study the effect of ocean acidification on algal motion in a more natural ocean setting, we investigated the average velocity of *Microglena* sp. induced by sunlight in a calm bay (Supplementary Figures 13). The horizontal and vertical sampling methods were consistent with the laboratory experiment, but the channel length was increased to 40 cm to ensure the stability of the equipment in seawater. The vertical channels were divided into two parts by rubber plug, the front part is 11 cm, the back part is 29 cm, and the latter part was injected with natural seawater to keep the tank stable. The horizontal channels were divided into two sections by acrylic spacers, the first section is 11cm, the second section is 29 cm, and the latter section was injected with natural seawater to keep the tank stable. In our experiment, we only used the front-

end 11 cm.

Flagellum shedding and regeneration. *Microglena* sp. was cultured to the exponential growth stage at the different pH values and then aeration was stopped. We used a Nikon Eclipse 80i microscope (Carl Zeiss, Inc., Thornwood, NY) to look at the flagella and calculated the percent of cells without flagella compared to total cells. pH-shocked cells were obtained by rapidly adding a large amount of culture medium saturated with CO_2 to the culture medium containing motile cells, centrifugation was conducted and medium with different acidification gradients was added. The proportion of flagellar regeneration was calculated by recording the motility of the cells.

Transcriptome. To explore the mechanism by which *Microglena* sp. responds to ocean acidification, on year 5 of the long-term experiment, the cultures of *Microglena* sp. "M400" and "M1000" were selected, centrifuged at 6 °C frozen in liquid nitrogen and stored at -80°C for subsequent transcriptomic (with three biological replicates for each sample) analysis. In order to avoid circadian bias, our sampling time was 6 hours after illumination, i.e. 14:00 h for all samples.

RT-PCR. RNA isolated from *Microglena* sp. (M400, M1000 and M2000) was treated with DNase I and then reverse-transcribed to cDNA using random hexamers. PCR was then performed using cDNA templates and primers specific for *Microglena* sp. genes MigICE16000, MigICE12547, MigICE10361, MigICE11569, MigICE4581, MigICE14893, MigICE8486, MigICE16283, MigICE4131, MigICE16837, MigICE5195, MigICE9498, MigICE14891, MigICE16200. Control PCR reactions were performed using chromosomal DNA templates and the same primer sets under the same PCR conditions. In order to avoid circadian bias, our sampling time was 6 hours after illumination, i.e. 14:00 h for all samples.

Calcium ions flux measurements. The net flux of Ca^{2+} between intracellular and extracellular was measured non-invasively using the scanning ion-selective electrode technique (SIET) (the SIET system, BIO-001A, Younger USA Sci. & Tech. Corp., Applicable Electronics Inc. and Science Wares Inc.). The measurements of the Ca^{2+} flux was performed as described by Sun *et al*. (2010) with some modifications [31]. The *Microglena* sp. cells were settled on the center of a poly-L-lysine-pre-treated cover slip and then placed in 4 ml of measuring solution (0.2 mM $CaCl_2$, 360 mM NaCl, 2.0 mM $NaHCO_3$, 8.0 mM KCl, 0.1 mM Na_2SO_4, 0.05 mM H_3BO_3, 0.5 mM NH_4NO_3, 2.0 mM Tris). Solution was pre-acidified at the corresponding pCO_2 before Ca^{2+} flux measurements. Three-dimensional ionic flux signals were continuously recorded for 5 min and plotted with MageFlux software that was developed by Xu Yue (http://xuyue.net/mageflux).

Distribution of *Microglena* sp. distribution and irradiance at different depths under melting ice. *Microglena* sp. live in the seawater beneath sea ice. Light intensity at the boundary of ice water increased to increase with the increase of external light intensity. When the light intensity exceeded the *Microglena* sp. saturation point, the algae moved downward to escape the strong light. When the light is lower than compensation point, the algae move upward to find the appropriate light intensity. We define the distance between compensation point and saturation point as distance of diurnal vertical movement (DVM). During a light cycle, *Microglena* sp. move up and down in seawater within the DVM. Light levels, which were attenuated by sea ice, were obtained from the formula $T=e^{-kb}$, T, extinction coefficient; e, Napierian base; k, constant; b, optical path[32]. The intensity of light decreases gradually with the thickness of sea ice due to the attenuation effect of sea ice on light. Light levels in sea water were obtained using data that we measured in the North Yellow Sea in October. Sea ice used in this experiment was artificially made from cold storage. After the natural seawater was filtered, the salinity was adjusted to 5 practical salinity units with

deionized water, and the temperature was lowered to -15 ℃ to obtain sea ice of different thicknesses.

Instantaneous velocity. Measurement of cell instantaneous velocity was based on the modified method of previous studies[30,32] using particle image velocimetry (PIV) (Stereo-PIV, TSI, USA)[30,32]. The container (side length 10 cm, opening above) was illuminated from one side by a laser sheet with a wavelength of 532 nm (the light that records the movement of cells). Phototactic responses of the cells were observed when the container was illuminated by LED light (SRZ-BLTO9W-01, GeShuo, China) from the top or side. The light intensity of light was 2 and 200 μmol photons·m^{-2}·s^{-1} at the top and side surface of the suspension. The illumination was slightly reduced as the depth within the vessel increased. In order to avoid the slightly non-uniform illumination effect, the brightness of the image at the same depth for the PIV analysis was measured. For *C. reinhardtii* and *D. salina*, the positive phototaxis-inducing light was 2 μmol photons·m^{-2}·s^{-1} and negative phototaxis-inducing light was 800 μmol photons·m^{-2}·s^{-1}.

The instantaneous velocity was calculated as follows:

Velocity = S /t (Equation 2)

S: displacement; t: move time = 1 s.

Statistical analyses. Each result that is shown is the mean of at least three biological replicates. Statistical analyses were performed using SPSS v.22 for Windows (SPSS, Chicago, IL, USA). Variance among treatments was tested using Kruskal Wallis test followed by Dunn's post-hoc test. The significance level was $P<0.05$ for all tests unless otherwise state.